Pramana – J. Phys. (2024) 98:122
https://doi.org/10.1007/s12043-024-02759-6

First-principle study of strontium intercalation in bilayer graphene

O FARKAD*, R TAKASSA, F ELFATOUAKI, S HASSINE, A EL MOUNCHARIH, O CHOUKRI, A OUAHDANI, E A IBNOUELGHAZI and D ABOUELAOUALIM

LaMEE, Department of Physics, Faculty of Sciences Semlalia, Cadi Ayyad University, P.O. Box 2390, 40000 Marrakech, Morocco
*Corresponding author. E-mail: omarfarkad@gmail.com

MS received 27 August 2022; revised 30 November 2023; accepted 23 January 2024

Abstract. Modifying electrical and optical properties in two-carbon materials is essential for electronic devices, energy storage and biosensor applications. We report a comparative study of the effect of systematically intercalated strontium atoms in AA- and AB-stacked bilayer graphene (BG) in the framework of density functional theory (DFT). The electronic band structures, the total and partial electronic density of states and the dielectric function are studied. We show that the intercalation of atoms can influence both electronic properties. Our results show that the Dirac cones, a signature of graphene, are translated into the conduction band. This property may be useful in band-gap tuning applications of nanodevices. The optical properties were calculated parallel and perpendicular to the graphene sheet under polarised electric fields. The calculated optical properties show that the intercalation of Sr in the AA- and AB-stacked BGs promotes IR absorption. The findings provide a basis for developing graphene intercalary compounds, which can be used in optoelectronics to control the absorption of light wavelengths and specifically in biosensor applications.

Keywords. Biosensor; Strontium; AA- and AB-stacked bilayer graphene; electronic properties; optical properties; density functional theory.

PACS Nos **78.67.Wj; 73.22.Pr; 71.15.Mb**

1. Introduction

Recent research has been at the forefront of developments in the field of biosensors, allowing them to be improved mechanically, electrochemically, optically and magnetically with high-performance arrays, which offer the possibility of stimulating innovations in biosensors [1,2]. Due to high sensitivity, size reduction and fast response time, biosensor research and development have attracted lots of attention [3]. Developing next-generation treatments, like personalised therapy and ultrasensitive point-of-care marker detection, is facilitated by highly selective biosensors, analytical tools that transform biological reactions to electrical signals [4–6].

Strontium is one of the trace elements with characteristics close to those of calcium and magnesium (group II of the periodic table). The characteristics of strontium make it useful in many areas of medicine [7], including bone regeneration [8–12], dentistry [13–17] and drug delivery [18–22]. It is employed in various fields, such as treatment of diabetes [21,23–28] and effective immunotherapy [29]. It is widely used in several applications, including biosensors, thanks to its diverse chemical and physical characteristics and applications as capacitors and catalysts in electronics [30,31]. Looi *et al* [32], by comparing the glycoproteins CA125 and SCC-Ag, specifically detected an integrated digital electrode (IDE) surface modified with strontium oxide. Researchers could determine whether they had found the right biomarker for uterine cancer. Wang *et al* [33] specifically used strontium oxide to detect SCC-Ag for surface functionalisation. The predetermined strontium oxide surface was formed on IDEs that had been immobilised with SCC-Ag antibodies to produce a sensor that could provide high-performance detection, significant scalability and lack of corrosion.

In this regard, our study's main goal is to compare the effects of strontium atom intercalation on the electronic and optical characteristics of AA- and AB-stacked bilayer graphene (BG) for biosensor application.

Graphene is the allotrope of carbon that has attracted a lot of interest from researchers in various fields [34],

Published online: 23 August 2024

due to its intriguing physical characteristics, including its massless electrons [35], high carrier mobility [36] and optical transparency [37].

Intercalation is the inclusion of an atom or group of atoms to modify a structure. The characteristics of a material, such as structure, electronics, optics, magnetism and transport [38–44] can be changed by changing a single atom or group of atoms. Li-intercalated BG in the AB and AA stacks was studied by Zhu *et al*. They found that bilayer graphene with an AA stack is more suitable for lithium storage. The former will transform into the latter with a particular concentration of intercalated lithium ions [45].

Sugawara and colleagues [39] disclosed the creation and characterisation of Li-intercalated BG in the Japanese research group's paper. The Li atoms placed on the BG are fully ionised and are evenly distributed between two close graphene layers. They demonstrated that the effective fabrication of Li-intercalated BG would enable the development of a nanoscale ionic battery. The role of intercalated atoms and their species in superconductivity is suggested by Ichinokura *et al* [40]. They revealed concrete proof of superconductivity at the thinnest limit of Ca-intercalated graphite, C_6CaC_6 bilayer graphene, while pure bilayer graphene and C_6LiC_6 exhibit non-superconducting behaviour.

Intercalation of atoms appears to be a useful technique for controlling heat transfer in two-dimensional materials, according to another work by Lu *et al* [43]. Due to their superconductivity, graphite intercalation compounds have garnered much attention. They use non-equilibrium molecular dynamics simulations to examine the heat transport in a bilayer intercalated with Ca (C_6CaC_6) atoms at normal temperatures. In terms of state occupancy and phonon frequency of metal ions, they examined the relevance of the start of superconductivity and its significance for metal-intercalated bilayer graphene by Kaneko and Saito [42]. They used first-principle calculations based on functional density theory to examine the energies and electronic structures of atoms of alkali metals (Li, Na, K, Rb and Cs) and alkaline earth metals (Be, Mg, Ca, Sr and Ba).

Yang *et al* [41] gave directions for examining the Na storage in graphene and hard carbon nanosheets. There has been much interest in Na-ion batteries as a cheap substitute for Li-ion batteries. BG is appealing for rechargeable batteries because of its distinctive features. This research indicates that faulty BG may be an option for the Na-ion batteries' negative electrode. Indeed, Sr atoms can be inserted into BG at several different locations, including the hole site (H) between the two ring hexagons, the bridge on the C–C bond, the top site on the C atom (T), the hybrid site (HT) where the Sr atom can be accommodated under the hexagonal ring of the upper C atoms and on top of a single C atom for the lower plane, and various other locations.

Therefore, the intercalation technique has been used to create new graphene intercalation compounds [46]. Exotic phenomena, including superconductivity, are exhibited by these molecules [47]. This procedure can provide graphene in low-dimensional systems with different electrical and magnetic characteristics [48]. Therefore, next-generation electronic devices, such as spin qubit devices [49] and spintronic devices [50], can utilise this modified graphene.

This work examines the structural, electronic and optical properties of the BG with intercalation of strontium atoms at the site H and the hybrid site (HT) for AA-stacked BG (AB-stacked BG, called the Bernal structure [51]), respectively, using first-principle calculations with the full potential linearised augmented plane (FP-LAPW) based on density functional theory (DFT). The present paper is organised as follows: This section presents the calculation method based on the DFT implemented on the Wien2K code. Section 2 explores the geometrical properties of our material according to the graphene bilayer's stacked mode. The numerical results and a detailed discussion are given in §3, while in §4, a summary and conclusions of our paper are presented.

2. Computational method

Using first-principle computations in the framework of the FP-LAPW wave [52,53] process executed on the Wien2k code [54,55], the volume optimisation is computed under the functional LDA, approximating exchange and correlation potential. We adopted the generalised approximation gradient (GGA) potential for the electronic and optical properties, precisely the PBE-GGA developed by Predew–Bruke–Enzrohoff [56–59]. The electronic configurations of our elements are C: [He]2 $s^2$2p^2, Sr: [Kr] 5 s^2. The core and valence state separation is defined by cut-off $R_{mt} * K_{\max}$, which was set to 6.0. The four crystalline structures under study are completely relaxed using the PORT method once the force on each atom reaches less than $2 \cdot 10^{-3}$ Ry/u.a. The basic dimension of the functions of the atomic orbitals, related to the angular momentum, has been fixed at $l_{\max} = 6$ as a maximum value. The base function is extended to $R_{mt} \times K_{\max} = 6$, where R_{mt} is the shortest atomic sphere radius and $K_{\max}$ is the biggest k vector in the plane-wave development. The Fourier development charge density is trimmed at $G_{\max} = 12$ (u.a.)$^{-1}$. In the first Brillouin zone (BZ), the K point number was set to 100, corresponding to 17 × 17 × 2 K point mesh. The iteration process ended when the total energy is 10^{-5} Ry or less.

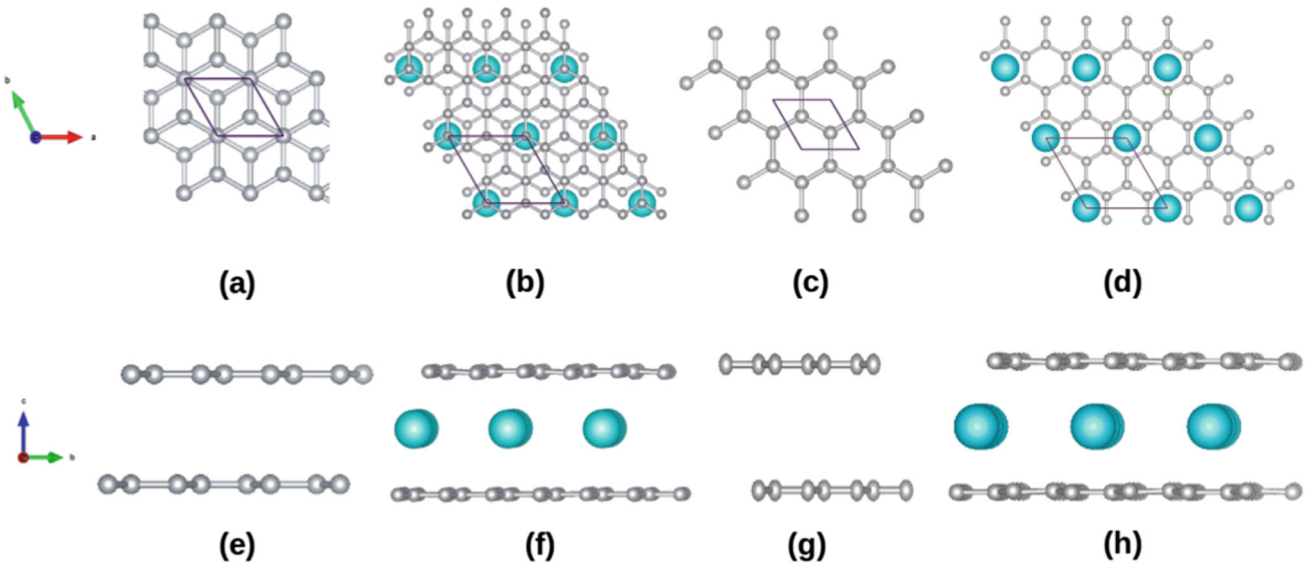

Figure 1. Top (**a**, **b**, (**c**,**d**)) and side (**e**, **f**, (**g**, **h**)) view of the AB(AA)-stacked BG and the Sr-intercalated AB(AA)-stacked BG systems, respectively, with gray indicating C and cyan indicating Sr atoms.

3. Results and discussion

3.1 *Structural properties*

To find out what strontium intercalation reveals about the structural, electronic and optical properties of AB- and AA-stacked BG, respectively, first we build a $2\times2\times1$ super-cell, which corresponds to a unit cell, containing eight independent carbon atoms, with 191(P6/mmm), (164($P\bar{3}m1$)) symmetry for AA(AB)-stacked BG as illustrated in figures 1a and 1b (figures 1e and 1f). Second, we intercalate the Sr atom into H and HT sites for AA- and AB-stacked BG, respectively. The unit cell of the intercalated systems contains nine independent atoms (see figures 1c and 1d, and 1g and 1h). The void between two BGs is retained at 10 Å to avoid interaction and to isolate the structure. The Murnaghan state equation (eq. (1)) is a useful tool for generating the energy–volume diagram shown in figure 2. This diagram can help with volume optimisation and relaxation, involving various structural parameters. These parameters include the bulk modulus (B), the first derivative of the bulk modulus (B'), the equilibrium unit cell volume (V_0) and the equilibrium energy (E_0). Additionally, it is noteworthy that the energy tolerance used in volume optimisation and relaxation is 10^{-4} Ry [60,61].

$$E(V) = E_0 + \frac{1}{14703.6}\left[\frac{BV}{B'}\left(\frac{(V_0/V)^{B'}}{B'-1}+1\right) - \frac{BV_0}{B'-1}\right]. \quad (1)$$

Table 1 summarises the optimised Murnaghan parameters of AB(AA)-stacked BG and Sr-intercalated AB(AA)-stacked BG. The relaxed parameters for the monolayer graphene are $a = b = 2.459585$ Å ($a = b = 2.459586$ Å) and the bond length d_{C-C} is 1.41 Å for both BGs. It agrees with other theoretical and experimental works, as shown in table 2 [62].

Moreover, the relaxed structure of the Sr intercalation AA(AB)-stacked BG system is SrC_{12} (SrC_6), in which an Sr atom has twelve (six) nearest neighbours, as shown in figures 1c, 1d (figures 1g, 1h). The C–C and C–Sr bond lengths are 1.42 and 2.38 Å (1.37 and 2.89 Å) for Sr intercalation AA(AB)-stacked BG. The interlayer distance between two graphene layers in Sr intercalation AA(AB)-stacked BG is 3.72 Å (3.75 Å), as shown in table 1. Because of the Sr intercalation, the C–C bond length is slightly (significantly) changed for AA(AB)-stacked BG. The not conservation and the conservation in the number of symmetry operations in the new structure of Sr intercalation in the AB- and AA-stacked BG reflect the modification in the symmetry of the intercalated material. It becomes only six rather than twelve operations for Sr-intercalated AB-stacked BG. This finding can be justified by the casualty of the inversion centre in the new pattern of Sr intercalation in the AB-stacked BG, which is chiral. In contrast, the Sr intercalation in the AA-stacked BG pattern is not chiral. It preserves its centre. The variation in the number of symmetry operations in the Sr-intercalated AB-stacked BG space group (156 (P3m1)) reflects changes in the symmetry, which the number of symmetry operations reduces to 6, compared to 12 in the

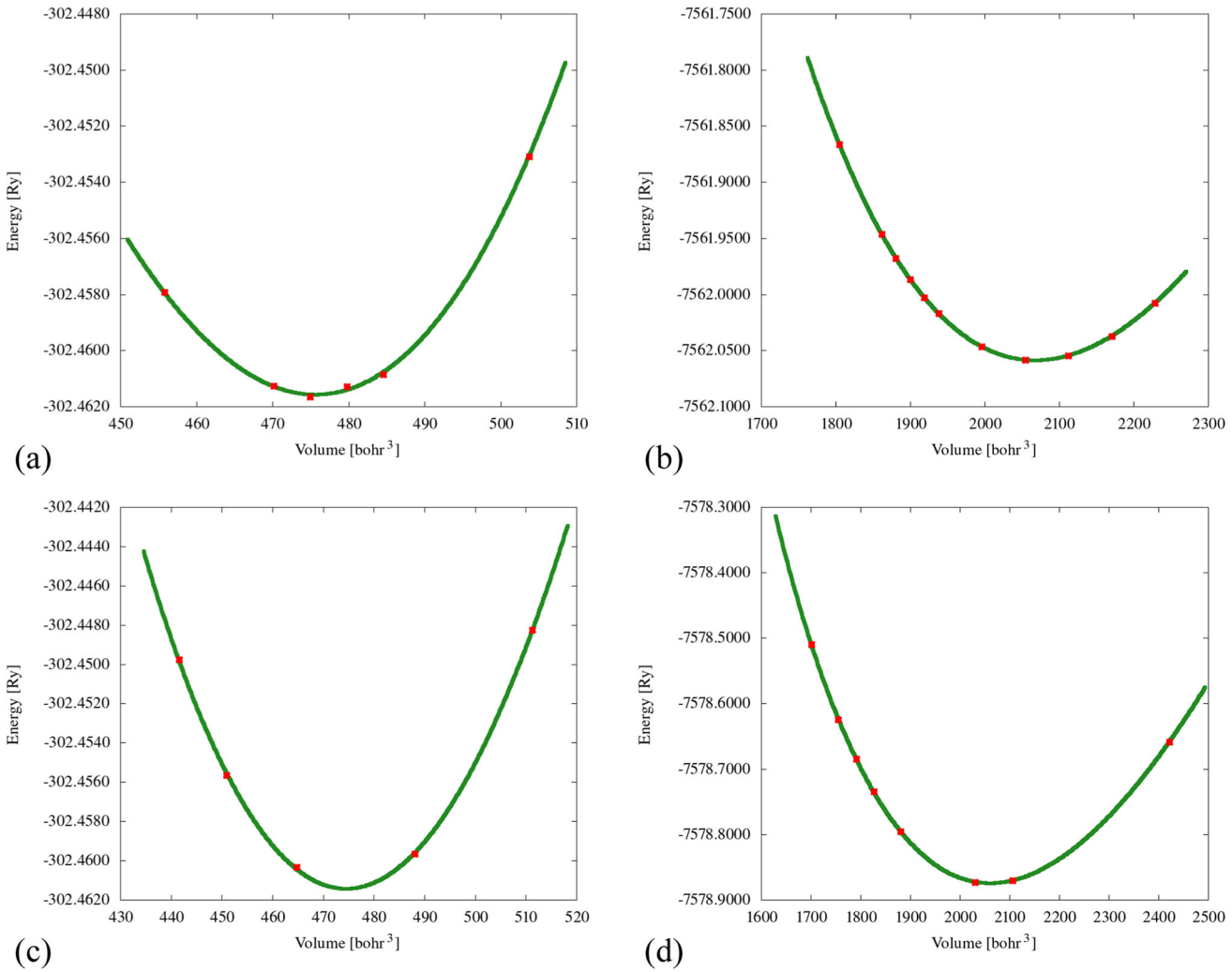

Figure 2. Energy–volume diagram of the AA(AB)-stacked BG (**a**, **c**) and the Sr-intercalated AA(AB)-stacked BG (**b**, **d**) materials.

Table 1. Optimised Murnaghan parameters of AB(AA)-stacked BG and Sr-intercalated AB(AA)-stacked BG materials, noted as AB-BG, AA-BG, Sr/AB-BG and Sr/AA-BG, respectively.

System	V_0 (bohr^3)	B (GPa)	B'	E_0 (Ry)
AB-BG	464.835	142.541	0.764	−302.460
AA-BG	475.711	137.302	−5.812	−302.461
Sr/AB-BG	2061.787	127.434	3.397	−7578.875
Sr/AA-BG	2068.214	135.510	3.732	−7562.060

AB-stacked BG (164 (P-3ml)). This can be attributed to the loss of the inversion center in the chiral pattern of Sr-intercalated AB-stacked BG. However, in Sr-intercalated AA-stacked BG, the symmetry operations remain unchanged from those of AA-stacked BG (191 (P6/mmm)) totaling 24.

Using total energy, we computed the formation energy per atom and the stability of the pure and intercalated structure was checked by utilising the following formula:

$$E_F = \frac{E_{BG} - 2 \times E_G}{N}, \tag{2}$$

where E_{BG}, E_G and N are the total energy of the BG, monolayer graphene and the total number of atoms in the AA(AB)-stacked BG, respectively. For the Sr-intercalated AA(AB)-stacked BG, the formation energy per atom is estimated as follows:

$$E_F = \frac{E_{IS} - (E_{BG} + E_{Sr})}{N}, \tag{3}$$

Table 2. Interlayer distance in BG, C–C and C–Sr bond lengths, space groups, formation energy per atom of AA(AB)-stacked BG and Sr-intercalatied AA(AB)-stacked BG materials, respectively.

	d_{G-G} (Å)		d_{C-C} (Å)				E_F (eV/at)	
Material	Cal.	Others	Cal.	Others	d_{C-Sr}	Space group	Cal.	Others
AB-BG	3.37	3.42[a], 3.225[b] 3.49[c]	1.41	1.420[a], 1.426[d]	– –	164 (P-3m1) –	−0.023	−0.020[b]
AA-BG	3.57	3.58[a], 3.525[b] – 3.65[c]	1.41	1.42[a], 1.426[d] –	– –	191 (P6/mmm) –	−0.024	−0.014[b]
Sr/AB-BG	3.7475	– –	1.3751 –	–	2.3809	156 (P3m1) –	−0.028	−0.034 (Li)[e] −0.031 (Ca)[e]
Sr/AA-BG	3.7245	–	1.4250		2.3449	191 (P6/mmm)	−0.128	−0.115 (Sr)[f]

[a]GGA implemented in the VASP code [71].
[b]Vanderbit implemented in the CASTEP code [41].
[c]Vanderbit based in the PHASE code [72].
[d]LDA implemented in the VASP code [45].
[e]LDA implemented in the CASTEP code [65].
[f]LDA implemented in the PHASE/0k code [42].

where E_{BG}, E_{Sr} and E_{IS} indicate the total energy of the pure BG, isolated Sr atom and the total energy of the intercalated material, respectively. Interlayer distance d_{G-G}, the C–C and C–Sr bond lengths, the space group and the formation energy E_F are indicated in table 2. We can deduce that Sr intercalation in the AA-stacked BG formation energy's per atom (−0.128 eV) is smaller than that in AB-stacked BG (−0.028 eV). So the structure of the Sr intercalation in the AA-stacked BG system is more stable than that in the AB-stacked BG system. Therefore, inserting the Sr atom at the site (H) for the AA-stacked BG is more suitable for the intercalation of Sr than AB-stacked BG because of its stability. This result is in good conformity with the previous studies on lithium [45,63–65].

3.2 *Electronic properties*

In the first step, based on FP-LAPW calculations in which the GGA-PBE functional was used for approximating the exchange-correlation potential, AA(AB)-stacked BG band's structure and Sr-intercalated AA(AB)-stacked BG structures are computed with 650 and 100 K points in the Brillouin zone, respectively. Electronic band structures are shown in figure 3. Figure 3a indicates that the band structure of AA-stacked BG presents a small gap due to the important Pauli repulsion between graphene layers, which suppresses electronic interlayer coupling. Figure 3c shows that the stacked bilayer AB has a band structure characterised by a double Dirac cone, where the valance and conduction bands connect in the K point [66–68]. Thus, at the Fermi level, the charge carriers behave as massless Dirac fermions, like in the case of graphene, a single sheet [69]. In addition, in the first Brillouin zone, at the high symmetry K point, the AA (AB) stacked BG has a gap equal to 0.243 eV (0 eV). Then AA(AB)-stacked BG has a semi-conducting (semi-metallic) behaviour, which agrees with the experimental data [70]. Furthermore, the band structure of the AA(AB)-stacked BG shows the same trend as the graphene monolayer at the high symmetry point Γ, where the gap at this point is 6.36 eV (6.43 eV), which introduces the characteristics of insulating materials. Similarly, the gap at the M point is almost 3.75 eV (3.78 eV). The band structure of Sr-intercalated AA(AB)-stacked BG are illustrated in figure 3b (figure 3d). It differs from AA(AB)-stacked BG mainly due to symmetry breaking. In the band structure diagram, we can see that the two Dirac cones, showing the linear dispersion bands, are separated by a small gap whose value is 0.08 eV (0.16 eV) at the Dirac K-point, under the Fermi level which are deposed in conduction band by 1.40 eV (1.33 eV), revealing the metallic nature of the Sr-intercalated AA (AB) stacking BG material [73]. This result is in agreement with the previous works for alkalis intercalated in BG and the single layer graphene's interaction with the substrate surface [74,75]. Thus, the intercalation process and the interlayer electronic coupling play significant roles in the modelling and formation of the band structure of graphene and its related materials [76].

The total and partial density of states (DOS) enclose a crucial role in specifying the electronic characteristics of the materials. Figures 4 and 5 show the partial and total DOS of the four materials under investigation. Figures 4a–4d show the total state densities (TDOS) of the AA(AB)-stacked BG and the intercalated materials viz, Sr-intercalated AA(AB)-stacked BG. Figure 4

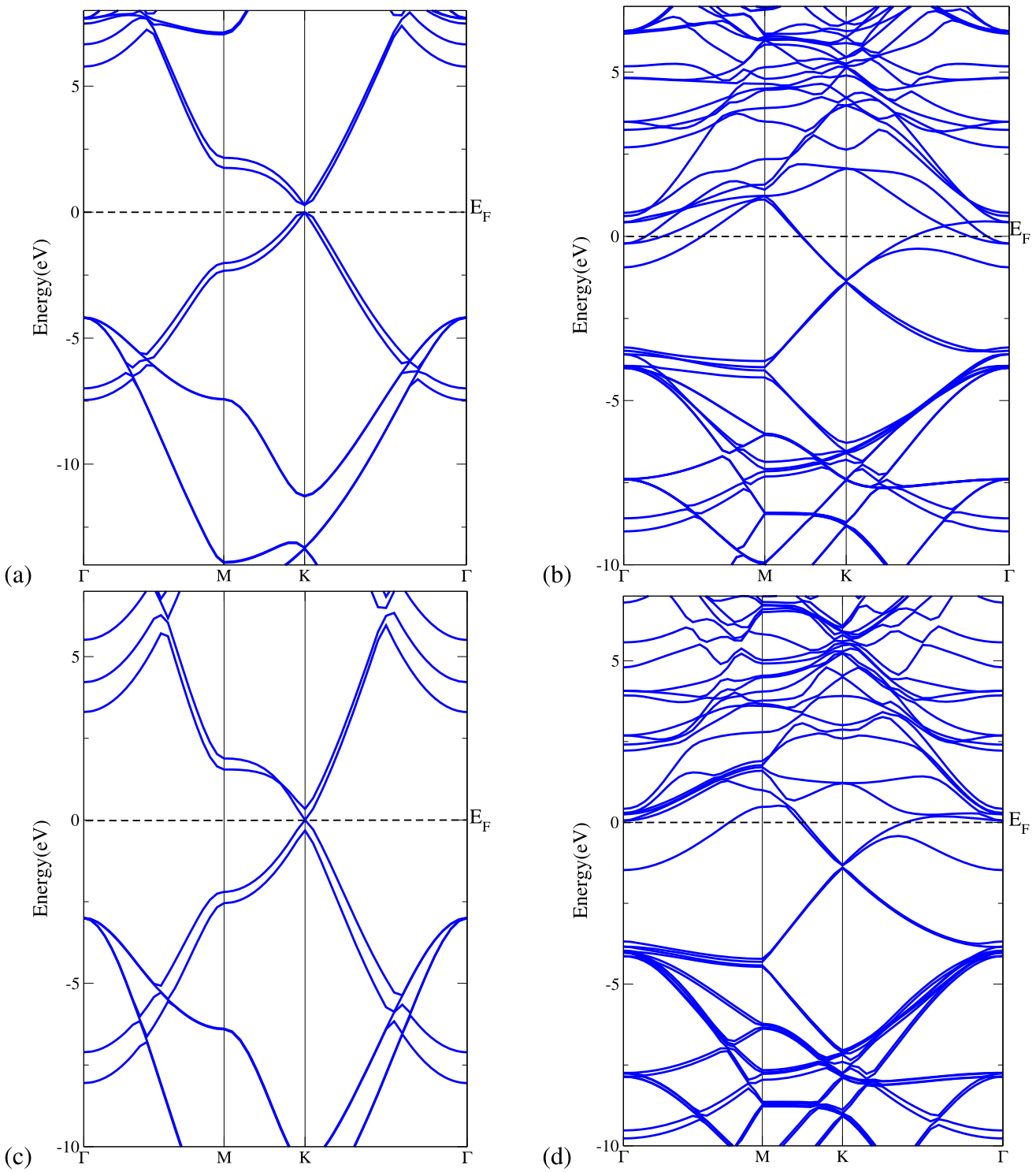

Figure 3. Band structure of the AA(AB)-stacked BG (**a**, **c**) and the Sr-intercalated AA(AB)-stacked BG (**b**, **d**) materials, respectively.

(figure 4c) shows the total density of states of the pure material AA(AB)-stacked BG with non-zero (zero) gap at the Fermi level. The gap equals 0.284 eV (0 eV) and this compound has semiconducting (semi-metallic) properties, affirming the band structure results. And it is nearly the temperament of C_p orbitals in the valence band and in the conduction band (notice figure 5a (figure 5d)).

The Sr atom intercalation modified DOS curves for both intercalated materials as indicated in figures 4 and

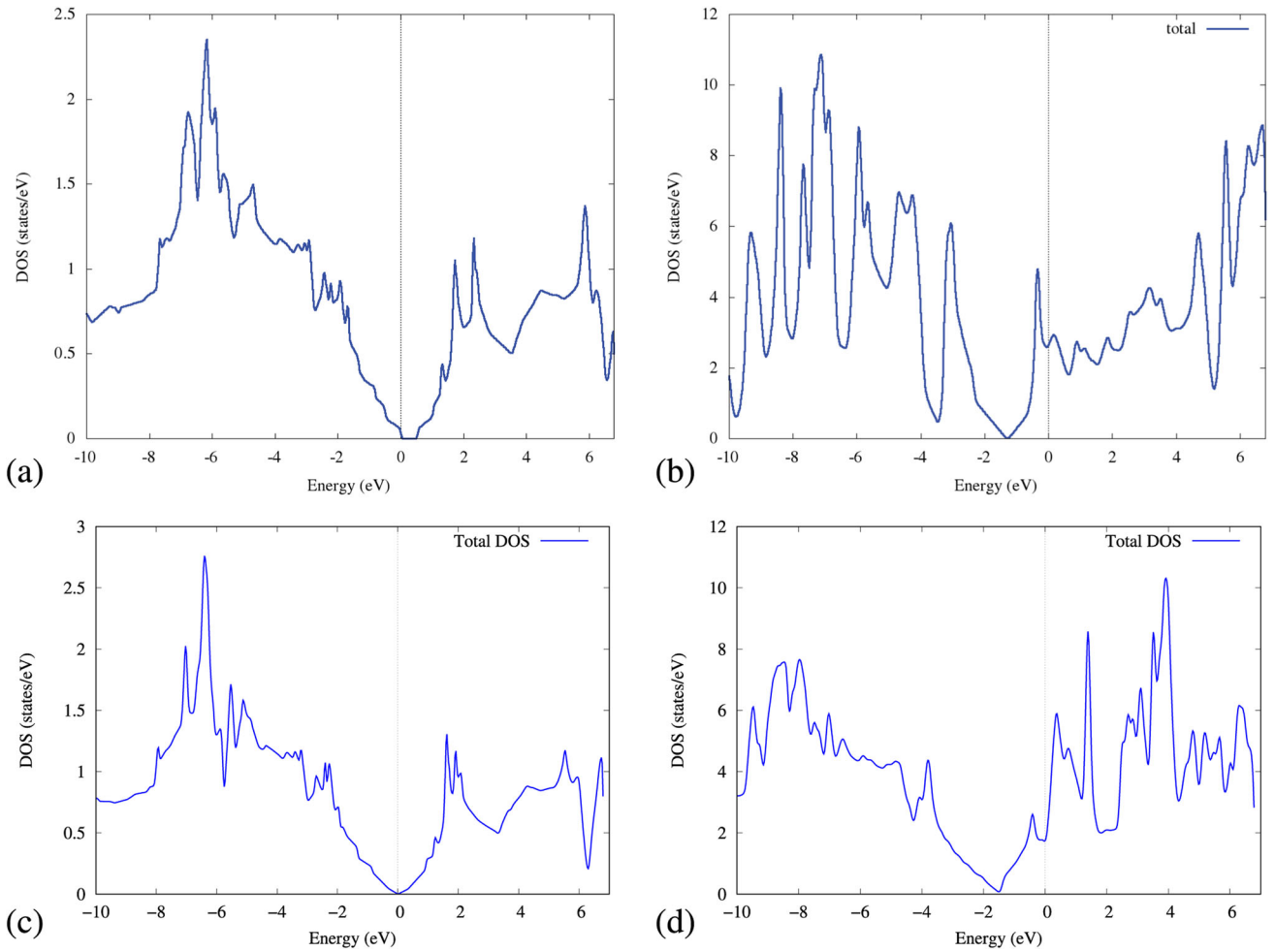

Figure 4. Total DOS of (**a**) AA-stacked BG, (**b**) AB-stacked BG, (**c**) Sr-intercalated AA-stacked BG and (**d**) Sr-intercalated AB-stacked BG.

5. It can be remarked that the Fermi level is shifted to the conduction band. Also, the creation of a small gap went to the left of the Fermi level (see figures 4b and 4d), conducting the change of the semi-conductor (semi-metallic) properties of pure AA(AB)-stacked BG to a metallic character for both intercalated materials. Moreover, as shown in figures 5e and 5f, the Sr intercalation into BG greatly improves the density of states at the Fermi level, which can be regarded as an expanded metallicity which is in accord with the results of Petrova and Yakovkin [74]. As shown in figures 5b, 5c, 5e and 5f, we can see that the p states of the C atoms are clearly encountered in the energy range from -10 to -2 eV. The energy range larger than 0 eV (conduction band) is dominated by the d states of the Sr atoms, demonstrating a robust interaction between these atoms.

Calculating the total valence charge density gives information about the chemical bonds between the different atoms forming the four systems, the pure BG and the intercalated structures. The electronic charge density in the (110) plane is shown in figure 6, which contains the C–Sr and the C–C bonds. The electronic charge distribution in figures 6b and 6d indicates that the C–C bond is a covalent type. At the same time, C–Sr is a covalent bond with a strong ionic character which can be justified by the presence of electron density isolines around the nuclei of the carbon atom. It can be explained by the fact that the bond between the alkali earth metal atom Sr and the non-metallic carbon atom C is of ionic character. At the same time, the different electronegativity makes the covalent bond weakly polar for the carbon atom.

The plots of the 3D and contour of the electron density of pure BG and Sr-intercalated AA(AB)-stacked BG are shown in figure 7. The contours of pure BG and interlayer materials are approximately similar to the previously calculated density charge distribution (see figures 7a, 7c and 7b, 7d). The 3D plot shows the presence of four peaks, corresponding to the charge accumulation on the four-carbon atomic sites, forming the basic unit of BG (see figures 7a and 7c). Five peaks are represented, which correspond to the charge accumulation on the carbon and strontium atoms that

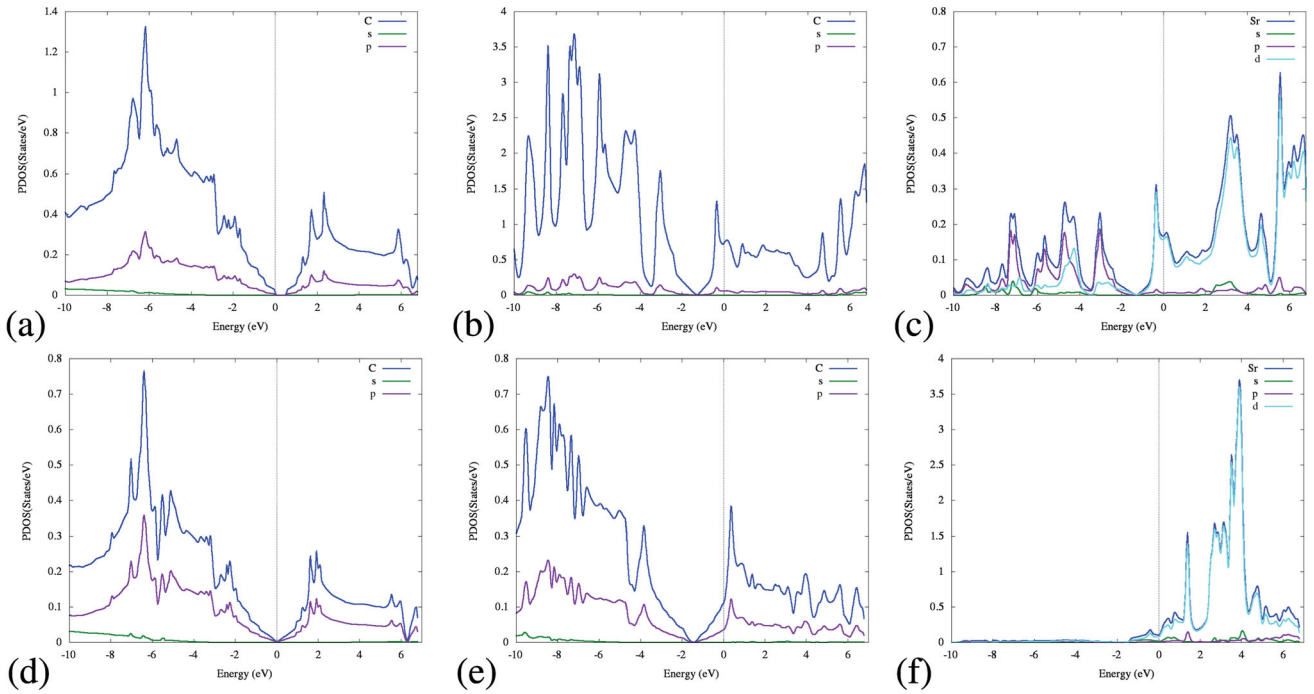

Figure 5. Partial DOS of pure AA(AB)-stacked BG (**a**, **d**) and Sr-intercalated AA(AB)-stacked BG (**b**, **c**, (**e**, **f**)).

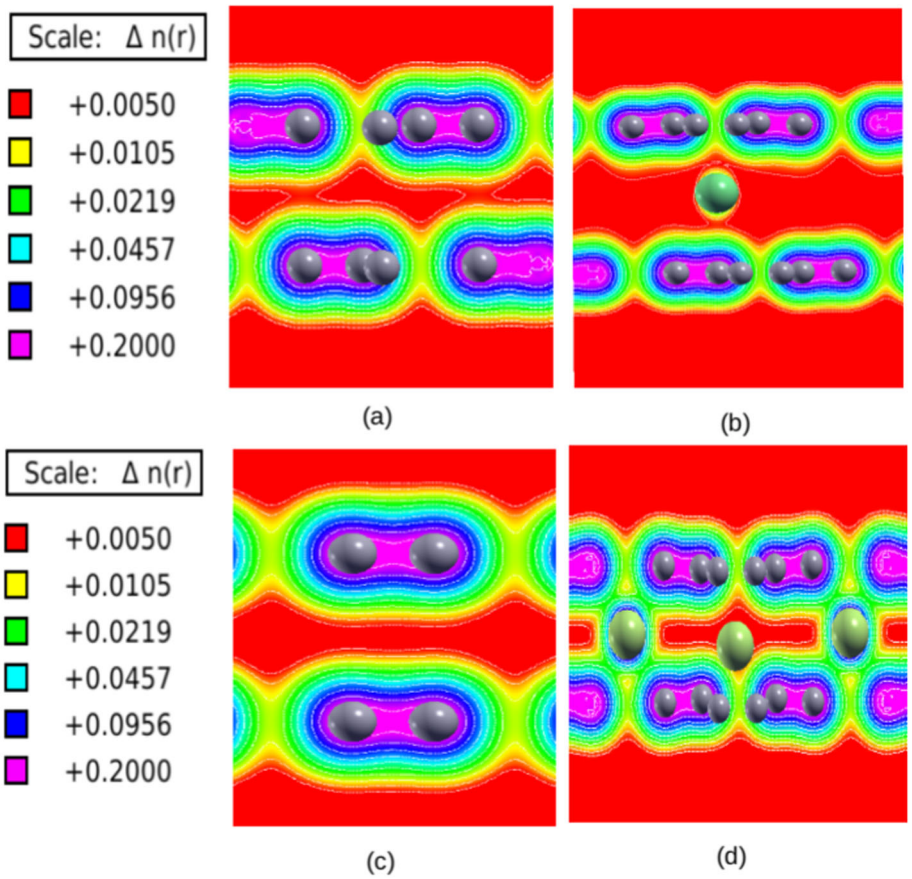

Figure 6. Electronic density plots. (**a**) AA-stacked BG, (**b**) Sr-intercalated AA-stacked BG, (**c**) AB-stacked BG, (**d**) Sr-intercalated AB-stacked BG, with gray indicating C and green indicating Sr atoms.

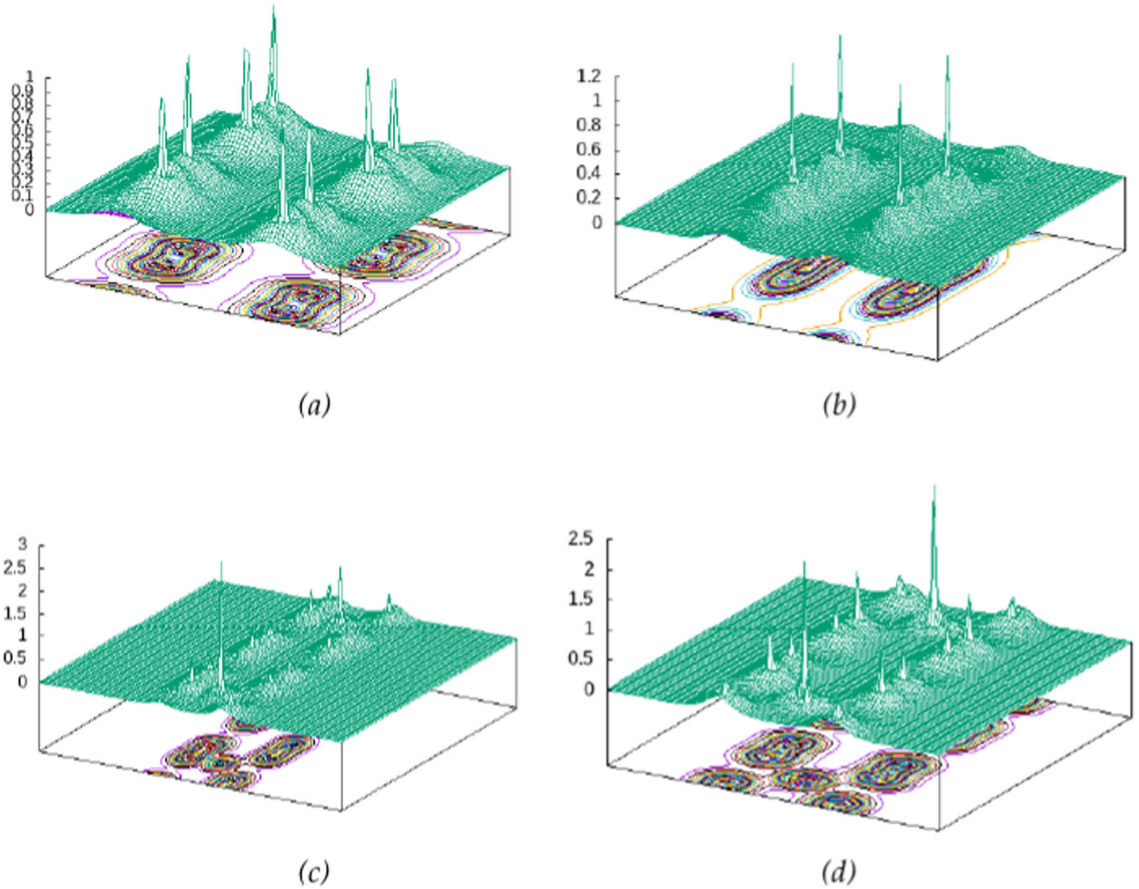

Figure 7. 3D electronic density plots. (**a**) AA-stacked BG, (**b**) Sr-intercalated AA-stacked BG, (**c**) AB-stacked BG and (**d**) Sr intercalated AB-stacked BG.

form the basic unit of the intercalated materials (see figures 7b and 7d).

The peak height indicates that the greatest accumulation of electrons is around the strontium atoms, which is expected because strontium atom has higher atomic number than carbon. Indeed, the concentration of electron density contours around carbon atoms is higher than around strontium atoms because the electronegativity of carbon (2.55 according to Pauling) is higher than that of strontium (0.95 according to Pauling). Therefore, for both intercalated systems, the 2D and 3D electron density analysis confirm that charge is efficiently transferred from Sr atoms to C atoms.

3.3 *Optical properties*

Calculations are made of the real and imaginary parts of the dielectric function, the absorption coefficient and the refractive index for polarisations perpendicular and parallel to the graphene plane for the pure AA(AB)-stacked BG and the Sr-intercalated AA(AB)-stacked BG materials. We used the Wien2k package's Random Phase Approximation Method (RPA), which was implemented by Gajdos, to carry out DFT simulations of the optical characteristics. The fundamental premise of the RPA approximation is based on the fact that the effects of the local electric field are completely ignored in favour of the transitions between the valence and conduction bands [77–79]. According to Brodersen, the dielectric tensor describes how materials react linearly to electromagnetic radiation [80].

3.3.1 *The dielectric function.* The dielectric function is a complex physical quantity. It is equal to the sum of the real and imaginary parts, as indicated by the following equation [81]:

$$\varepsilon(\omega) = \varepsilon_1(\omega) + i\ \varepsilon_2(\omega). \tag{4}$$

A denser K point mesh is required to precisely calculate the optical response qualities. Therefore, we have employed a wide mesh of 5000 K-points in the current calculations, equivalent to $27 \times 27 \times 6$. The Kramers–Kronig transformation can be used to determine the real part $\varepsilon_1(\omega)$ of the dielectric function $\varepsilon(\omega)$ because the

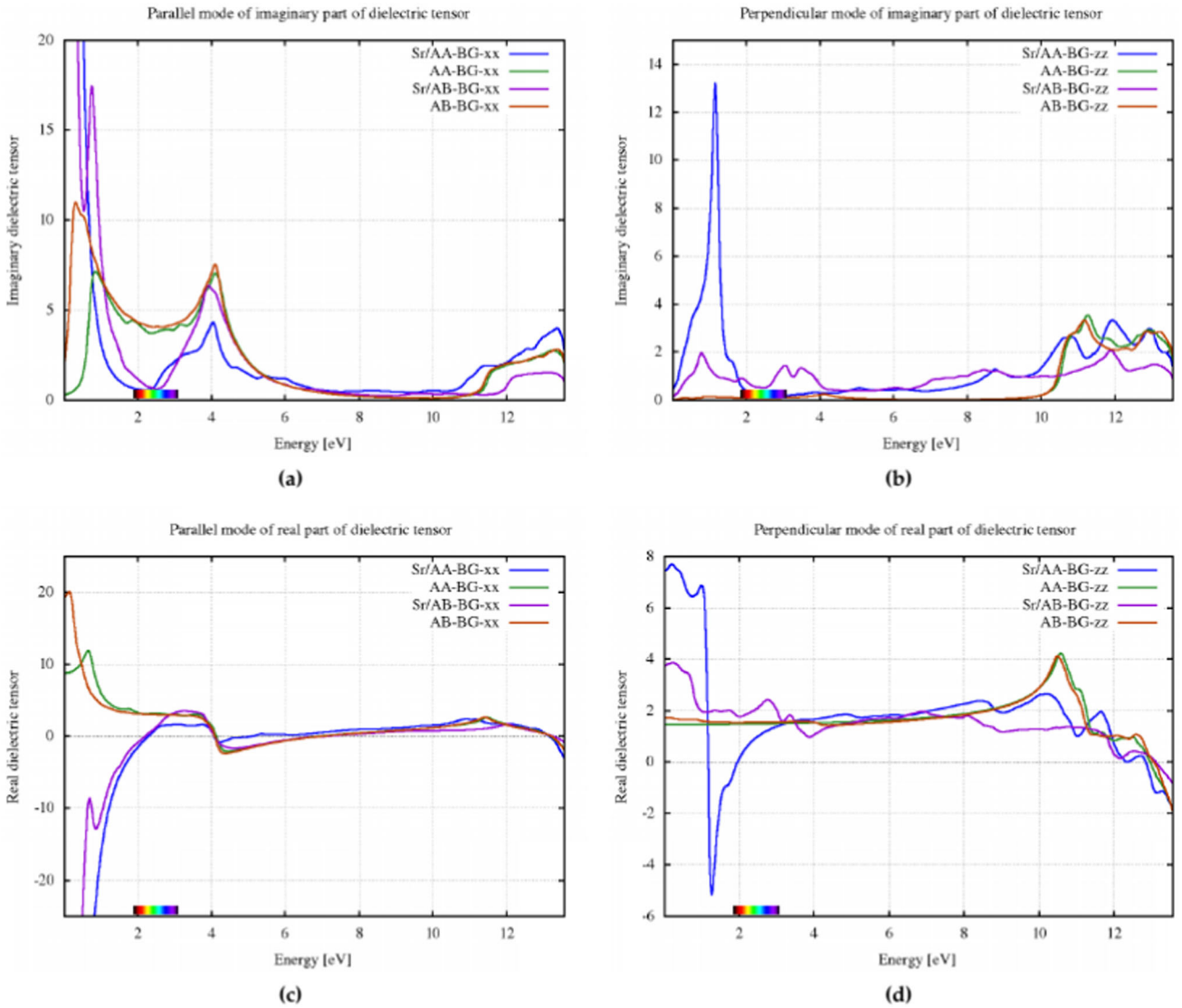

Figure 8. The imaginary (**a** and **b**) and real (**c** and **d**) parts of the dielectric function.

imaginary part $\varepsilon_2(\omega)$ relies on frequency:

$$\varepsilon_1(\omega) = 1 + \frac{2}{\pi} P \int_0^{\infty} \frac{\omega' \varepsilon_2(\omega')}{\omega'^2 - \omega^2} \mathrm{d}\omega', \tag{5}$$

where P is the principal value [77].

The isotropies of AA(AB)-stacked BG and Sr-intercalated AA(AB)-stacked BG along the *xx*- and *yy*-axes show only the optical functions in the *xx*- and *zz*-axes. Figures 8a and 8b (figures 8c and 8d) illustrate both the polarisation modes of the imaginary (real) part of the dielectric function when the polarisation is along the *xx*- and *zz*-axes, which are parallel ($\|$) and perpendicular ($\perp$) to the plane of graphene sheets. Figures 8a, 8b and 8c, 8d show that the dielectric function $\varepsilon(\omega)$ has anisotropic behaviour for two different polarisations, parallel ($E_{\|}$) and perpendicular ($E_{\perp}$), of the electric field.

From figure 8, we can see that $\varepsilon_2^{\|}(\omega)$ of AA(AB)-stacked BG are anisotropic for the two polarisations. It shows three mean peaks, at 0.77, 4.04 and 13.26 eV (0.31, 4.10 and 13.26 eV) formed by π to π^* and σ to σ^* transitions, respectively. Furthermore, in figure 8b, $\varepsilon_2^{\perp}(\omega)$ shows the same behaviour for both pure BG. It is practically zero all along the energy range, except at points 11.25 and 11.17 eV, where it shows a small peak, generated by σ to π^* transitions for AA(AB)-stacked BG material respectively. A small red-shift is observed for this peak, caused by the BG stacked type. Our results agree with previous theoretical works [82,83].

Table 3 shows the calculated values of the static dielectric constant along parallel and perpendicular directions. From these data, it can be seen that the $\varepsilon_2^{\|}(\omega = 0)$ of Sr-intercalation AA(AB)-stacked BG systems, is diverged. Thus, Sr-intercalated in the stacked

Table 3. The static dielectric constant values $\varepsilon(0)$.

System	$\varepsilon_2^{\parallel}(0)$	$\varepsilon_2^{\perp}(0)$	$\varepsilon_1^{\parallel}(0)$	$\varepsilon_1^{\perp}(0)$	$n_{\parallel}(0)$	$n_{\perp}(0)$
AA-stacked BG	0.25	0.00	8.60	1.90	2.96	1.21
AB-stacked BG	2.11	0.02	19.40	1.71	4.40	1.30
Sr-intercalated AA-stacked BG	$+\infty$	0.45	$-\infty$	7.44	$+\infty$	2.58
Sr-intercalated AB-stacked BG	$+\infty$	0.16	$-\infty$	3.76	$+\infty$	2.39

BG AA(AB) behaves like a metallic material according to the Drude model. In effect, $\varepsilon_2^{\parallel}(\omega)$ diverges at zero energy and decreases rapidly due to the energy loss associated with the DC electrical resistivity of metals [84].

In addition, in figure 8 the imaginary part $\varepsilon_2^{\parallel}(\omega)$ of the Sr-intercalated AA-stacked BG shows one peak in the ultraviolet B light (UVB) (3.94−4.43 eV), while the Sr-intercalated AB-stacked BG shows two major peaks, the first in the short-wave infrared (SWIR) range (413–886 meV) and the second occurs in the ultraviolet B light (UVB) (3.94−4.43 eV).

Furthermore, from figure 8b we can see that the perpendicular polarisation properties of the dielectric function $\varepsilon_2^{\perp}(\omega)$ for the Sr-intercalated AA-stacked BG are very different from those of the Sr-intercalated AB-stacked BG and of the pure BG. It has a master peak at lower energy, around 1.00 eV. Therefore, the Sr-intercalated AA-stacked BG has high absorbing properties in the IR region. It will be a good cancer therapy agent using IR sources [85]. At the same time, It presents two double peaks at 10.63, 10.84 eV and 11.93, 12.94 eV. Moreover, $\varepsilon_2^{\perp}(\omega)$ of Sr-intercalated AB-stacked BG presents two master peaks at 0.83 and 11.80 eV.

The dielectric function's real part $\varepsilon_1(\omega)$ is shown in figures 8c and 8d for all systems studied. From table 3, it can be noted that the static values of the real part $\varepsilon_1^{\parallel}(0)$ along the x-axis increase for the pristine BG when changing from AA- (8.60) to AB-stacked (19.40). It diverged for the two intercalated compounds. So, both Sr intercalation in the AA- and Sr-intercalation in the AB-stacked BG demonstrated purely metallic behaviour. Also, $\varepsilon_1^{\parallel}(\omega)$ has positive values for the spectra of AA- and AB-stacked BG. While it takes negative values for Sr intercalation in the AA and Sr intercalation in the AB-stacked BG from 0 to 2.27 eV (IR spectrum), it started to have positive values and behaves almost the same for all four materials. Contrary to the Sr intercalation in the AA-stacked BG, it should be noted that $\varepsilon_1^{\parallel}(\omega)$ of the Sr intercalation in the AB-stacked BG shows an anomalous variation, where it manifests a small oscillation in the energy range (0.63−0.77) eV, and such observation is still unclear. Thus, the intercalation of Sr in BG enhances the absorption phenomena in the IR region.

In addition, from table 3, in perpendicular mode, the static values of the real part $\varepsilon_1^{\perp}(0)$ increased. When we move from AA- to AB-stacked BG, the Sr intercalation keeps this tendency and rather consolidates. Indeed, $\varepsilon_1^{\perp}(0)$ of the Sr-intercalation in the AA-stacked BG (7.44) is almost twice as large as the Sr intercalation in the AB-stacked BG (3.76). From figure 8d, we can see that $\varepsilon_1^{\perp}(\omega)$ has positive values for the spectra of all ours systems in (0.0−1.16) eV range, where $\varepsilon_1^{\perp}(\omega)$ exhibits a mean peak at 0.2 eV. Then the materials have a transparent behaviour in (0.0−1.16) eV. After this energy range, only Sr intercalation AA-stacked BG switched to an opaque behaviour (1.16−1.94) eV, where $\varepsilon_1^{\perp}(\omega)$ takes a negative value. The same behaviour is attributed to all our systems in the (12.85−13.57) eV range corresponding to the edge of the extreme ultraviolet spectrum (10.25–124) eV. On the other hand, since $\varepsilon_1^{\perp}(\omega)$ takes positive values in (1.97−12.83) eV, AA-stacked BG, AB-stacked BG, Sr-intercalated AA-stacked BG, Sr-intercalated AA-stacked BG show transparent behaviour. Moreover, it should be noted that the master peaks in this scale revert to the two pristine BG. The Sr-intercalated doses also improve the absorption of BG in IR and the extreme ultraviolet spectrum.

3.4 *The refractive index*

3.4.1 *The static refractive index.* One of the most crucial variables in the real portion of the dielectric function is the static refractive index, indicated by the symbol $n(0)$. It can be computed using the real part of the dielectric function when the frequency of the incident light reaches zero, which is given by

$$n(0) = \sqrt{\varepsilon_1(0)}. \tag{6}$$

The computed values of the static refractive index in parallel and perpendicular directions are shown in table 3. The results show that the intercalation significantly affects the values of this parameter. It can be seen that the static refractive index changes with change in the direction of polarisation for all the structures. In the case of the intercalated systems, this parameter becomes infinite in the parallel direction confirming metallic behaviours

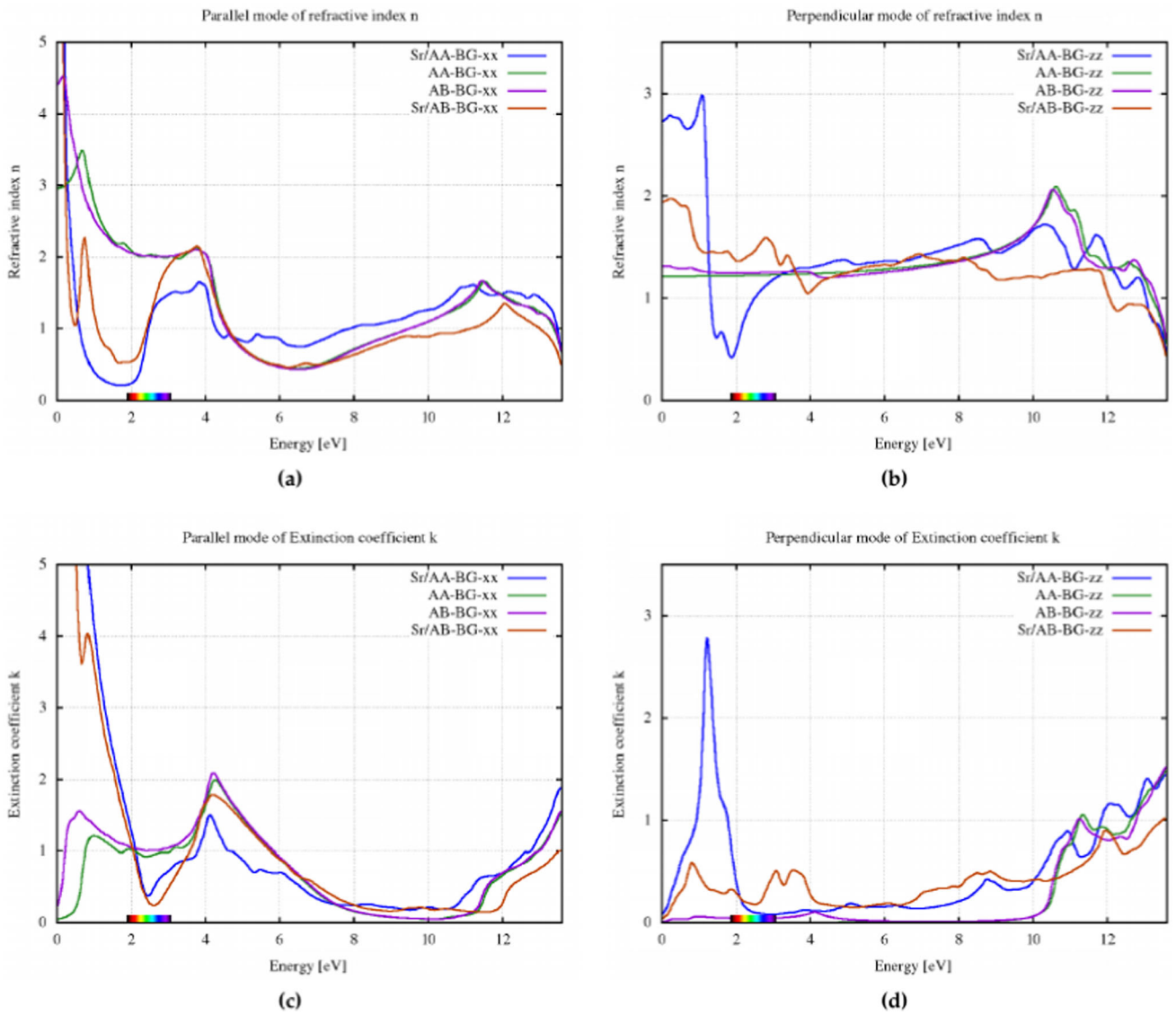

Figure 9. The refractive index (**a** and **b**) and extinction coefficient (**c** and **d**).

of Sr-intercalated AA- and Sr-intercalated AB-stacked BG.

3.4.2 *The refractive and extinction coefficients.* The difference between an electromagnetic wave's travel through a vacuum and another substance is described by the complex refractive index, $N(\omega)$. It is calculated using the following relationship:

$$N(\omega) = n(\omega) + ik(\omega). \tag{7}$$

Moreover, in optical devices, the potential applications of optical materials require a proper knowledge of the refractive index $n(\omega)$ and extinction coefficient $k(\omega)$, which are directly related to the absorption of the material. They are calculated using the values of $\varepsilon_1(\omega)$ and $\varepsilon_2(\omega)$:

$$n(\omega) = \sqrt{\frac{|\varepsilon(\omega)| + \varepsilon_1(\omega)}{2}}, \tag{8}$$

$$k(\omega) = \sqrt{\frac{|\varepsilon(\omega)| - \varepsilon_1(\omega)}{2}}. \tag{9}$$

Here $|\varepsilon(\omega)| = \sqrt{\epsilon_1(\omega)^2 + \varepsilon_2(\omega)^2}$ is the modulus of dielectric function. The spectra of the refractive index $n(\omega)$ and the extinction coefficient $k(\omega)$ are shown in figures 9a, 9b and figures 9c, 9d, respectively. The results show the anisotropic behaviour of $n(\omega)$ and $k(\omega)$ and the Sr intercalation significantly affect the optical response.

From figures 9a and 9b, it can be seen in the IR energy range that the refractive index in both polarisation directions of the AB-stacked BG structure is greater than AA-stacked BG. It has the same behaviour in most of

Table 4. Energies, polarisation states and spectral region of the refraction coefficient peaks of AA (AB)-stacked BG, Sr-intercalated AA (AB)-stacked BG.

Material	Peaks ∥	Peaks ⊥	Energy (eV)	Spectrum region
AA-stacked BG	3.49	–	0,67	IR
	2.13	–	3.74	Visible
	–	2.10	10.6	UV
	1.66	–	11.5	UV
	1.27	–	0.53	IR
	2.11	–	4.20	UV
AB-stacked BG	–	1.10	11.22	UV
	–	1.52	13.6	UV
Sr-intercalated AA-stacked BG	–	2.65	0.18	IR
	1.71	–	3.82	Visible
	–	1.38	4.86	UV
	1.61	–	11.22	UV
	2.33	–	0.83	IR
Sr-intercalated AB-stacked BG	1.70	–	4.18	UV
	–	0.57	0.83	IR
	–	0.32	1.89	Red

the energy range in the two directions of polarisation. After the Sr intercalation, the results show that for the Sr-intercalated AA- and Sr-intercalated AB-stacked BG, the value of refractive index shifts to the positive infinite value at the IR region in the *xx* direction, confirming the metallic behaviour in this direction. In contrast, in the *zz* direction, the refractive index in the IR region increases up to 2.75 and 1.9 for Sr-intercalated AA-stacked BG and Sr-intercalated AB-stacked BG, respectively, indicating semiconducting behaviour.

We also observe the appearance of several peaks in both polarisation directions (figures 9a and 9b). Among these peaks, we can cite for Sr-intercalated AA-stacked BG structure, two sharp peaks (1.6 and 1.7) at the UV region in the *xx* direction and one intense peak (3.0) at the IR region in the *zz* direction. For Sr-intercalated AB-stacked BG we can see two intense peaks (2.3 and 2.2) at the IR and UV region, respectively in the *xx* direction and one intense peak (2.95) at the IR region in the *zz* direction. For pure and intercalated structures, however, the refractive index value decreases to less than one after exposure to various energy levels in both polarisation directions, resulting in photoluminescence phenomenon (where the phase velocity of the passing light is faster than the speed of light in vacuum).

The extinction coefficient is plotted in figures 9c and 9d. It clearly shows the anisotropic behaviour of this parameter and follows almost the same behaviour of the absorption coefficient. Before the Sr intercalation in the *xx* direction, the extinction coefficient presents two intense peaks, 1.2 and 2.0 (1.5 and 2.1) for the AA(AB)-stacked BG system at the IR and UV energy ranges, respectively, indicating the lowest transmission and maximum absorption of light in this region. At the same time, in the *zz* direction, the extinction coefficient is almost zero at all energy ranges (0–10 eV), indicating that before intercalation, the structures do not attenuate most of the incident light. Then this parameter increases after 10 eV. Electromagnetic waves hardly pass through these materials after this threshold.

After the intercalation, it can be seen in the *xx* direction (figure 9c), that the extinction coefficient value is infinite for intercalated structures at the IR energy region, indicating the lowest transmission and maximum absorption of the incident light and decreases to reach its minimum at the green light region. Therefore, these structures will not attenuate most of the incident visible light. We can also see an increase in the extinction coefficient in the UV range, especially (3.5−4.5 eV), which means the light transmission is the lowest in this region.

In the *zz* direction (figures 9d), the maximum value of the extinction coefficient (2.75) appears for the Sr-intercalated AA-stacked BG system at the IR region (1−1.5 eV), indicating an attenuation of the incident light while for Sr-intercalated AB-stacked BG system reaches one maximum peak (0.5) at the IR region indicating a weak attenuation of the incident light. This result is promising for photothermal therapy based on the use of a photoabsorbent in the near-infrared (NIR) region. Such methodology has proven to be effective for the local treatment of cancer [85]. In addition, we can observe an increase in the extinction coefficient at the UV energy region (10–14 eV) for two intercalated systems, where the lowest transmission occurs. Finally, all peaks observed are tabulated in table 4.

4. Conclusion

The impact of alkaline metal Sr atom intercalation on the structural, electrical and optical characteristics of the AA- and AB-stacked BG was examined using the density functional theory (DFT) computations. The Sr-intercalated AA- and Sr-intercalated AB-stacked BG crystallise respectively in the hexagonal system with the SrC 12 and SrC6 structure type and are more energetically stable than pure BG, according to relaxation results and the calculated formation energy. After Sr atom intercalation, the electronic properties of AA- and AB-stacked BG change from a semiconductor with a small gap and semi-metallic with no gap to pure metallic behaviour. The Dirac cones in Sr-intercalated AA- and Sr-intercalated AB-stacked BG are approximately 1.38 and 1.33 eV under the Fermi level, respectively. The accumulation of electrons is maximal around the strontium atoms, indicating an efficient transfer of electric charges from the strontium atom to the carbon atoms. It has consequences on the transport of graphene intercalation compounds. Additionally, the behaviour of all optical parameters, including the dielectric function, refractive and extinction coefficients, is anisotropic. After the Sr atom was intercalated, the static refractive index decreased for parallel polarisation and increased for perpendicular polarisation. After exposure to various energy levels in both polarisation directions, the refractive index decreases to below one, leading to the occurrence of photoluminescence phenomena for both pure and intercalated systems. Beside, the imaginary part's value and extinction coefficient show sharp peaks in the vertical mode at the IR spectrum. The findings of this study provide a foundation for creating graphene Sr intercalation compounds for cell cancer biosensing, optoelectronic nanodevices and battery electrodes.

References

[1] Z Hua, T Yu, D Liu and Y Xianyu, *Biosens. Bioelectron.* **179**, 113076 (2021)
[2] R Nagraik, A Sharma, D Kumar, S Mukherjee, F Sen and A-P Kumar, *Sens. Int.* **2**, 100089 (2021)
[3] A Kawamura and T Miyata, *Biomater. Nanoarchitecton.* 157 (2016)
[4] A Gosai, K-R Khondakar, X Ma and M-A Ali, *Biosensors* **11**, 384 (2021)
[5] H-A Alhadrami, *Biotechnol. Appl. Biochem.* **65**, 497 (2018)
[6] P Parkhey and S-V Mohan, *Microb. Electrochem. Technol.* **2019**, 977 (2019)
[7] S Mukherjee and M Mishra, *Nanotechnol. Environ. Eng.* **6**, 25 (2021)
[8] P-J Marie, P Ammann, G Boivin and C Rey, *Calcif. Tissue Int.* **69**, 121 (2001)
[9] S-C Verberckmoes *et al*, *Kidney Int.* **64**, 534 (2003)
[10] E Gentleman, Y-C Fredholm, G Jell, N Lotfibakhshaiesh, M-D O'Donnell, R-G Hill and M-M Stevens, *Biomaterials* **31**, 3949 (2010)
[11] K Qiu *et al*, *Biomaterials* **27**8, 1277 (2006)
[12] W Li, Y Hu, L Shi, X Zhang, L Xiong, W Zhang and I Ullah, *J. Biomater. Sci.* **29**, 1155 (2018)
[13] K Zhao, Q Feng and G Chen, *Tsinghua Sci. Technol.* **4**, 1570 (1999)
[14] S Narisawa, N Fröhlander and J-L Millán, *Dev. Dyn.* **208**, 432 (1997)
[15] N-B Watts, *Clin. Chem.* **45**, 1359 (1999)
[16] Y Chen, A Gao, L Bai, Y Wang, X Wang, X Zhang and P-K Chu, *Mater. Sci. Eng. C* **75**, 1049 (2017)
[17] V-E Carvalho, D-M De Paula, A-D Neto, L-S Costa, D-F Dias, V-P Feitosa and P-B-A Fechine, *J. Mech. Behav. Biomed. Mater.* **101**, 103447 (2020)
[18] N Khamsehashari, S-A Hassanzadeh-Tabrizi and A Bigham, *Mater. Chem. Phys.* **205**, 283 (2018)
[19] M Filippousi, P-I Siafaka, E-P Amanatiadou, S-G Nanaki, M Nerantzaki, D-N Bikiaris and G Van Tendeloo, *J. Mater. Chem. B* **3**, 5991 (2015)
[20] C Zhang *et al*, *Biomaterials* **31**, 3374 (2010)
[21] F-A Kiani, U Shamraiz, A Badshah, S Tabassum, M Ambreen and J-A Patujo, *Artif. Cells, Nanomed. Biotechnol.* **46**(sup3), 1083 (2018)
[22] W-Y Qian, D-M Sun, R-R Zhu, X-L Du, H Liu and S-L Wang, *Int. J. Nanomed.* **7**, 5781 (2012)
[23] K Kasirajan and M Karunakaran, *Sens. Lett.* **17**, 924 (2019)
[24] Y Lin, Z Yang, J Cheng and L Wang, *J. Wuhan Univ. Technol.-Mater. Sci. Ed.* **23**, 475 (2008)
[25] A Rothschild, W Menesklou, H-L Tuller and E Ivers-Tiffee, *Chem. Mater.* **18**, 3651 (2006)
[26] Z Mao *et al*, *Front. Pharmacol.* **9**, 368 (2018)
[27] G Apsana, P-P George, N Devanna and R Yuvasravana, *Asian J. Pharm. Clin. Res.* **11**, 384 (2018)
[28] G-L Cao *et al*, *Med. Sci. Monit.* **24**, 6525 (2018)
[29] M Garbani *et al*, *Allergy* **72**, 570 (2017)
[30] M-M Rahman, M-M Hussain and A-M Asiri, *RSC Adv.* **6**, 65338 (2016)
[31] M Kim *et al*, *Ceram. Int.* **42**, 17853 (2016)
[32] M-L Looi, M-A-Z Hatta, M-S Aishah, M-H Baizurah, W-W Zurinah and M-Y Anum, *Int. J. Cancer Res.* **2**, 212 (2006)
[33] H Wang, T Lakshmipriya, Y Chen and S C Gopinath, *Biomed. Res. Int.* **1**, 2807123 (2019)
[34] A Gupta, T Sakthivel and S Seal, *Prog. Mater. Sci.* **73**, 44 (2015)
[35] S S Kubakaddi, *Phys. Rev. B* **79**, 075417 (2009)
[36] M-A Brown, M-S Crosser, M-R Leyden, Y Qi and E-D Minot, *Appl. Phys. Lett.* **109**, 093104 (2016)
[37] Z Qiao *et al*, *Sci. Rep.* **5**, 14441 (2015)
[38] M-S Dresselhaus, *Phys. Today* **37**, 60 (1984)
[39] K Sugawara, K Kanetani, T Sato and T Takahashi, *AIP Adv.* **1**, 022103 (2011)

[40] S Ichinokura, K Sugawara, A Takayama, T Takahashi and S Hasegawa, *ACS Nano* **10**, 2761 (2016)
[41] S Yang, S Li, S Tang, W Dong, W Sun, D Shen and M Wang, *Theor. Chem. Acc.* **135**, 1 (2016)
[42] T Kaneko and R Saito, *Surf. Sci.* **665**, 1 (2017)
[43] S Lu, Y Ouyang, C Yu, P Jiang, J He and J Chen, *J. Appl. Phys.* **129**, 225106 (2021)
[44] O Farkad, R Takassa, F Elfatouaki, S Hassine, Y Ijdiyaou, E A Ibnouelghazi and D Abouelaoualim, *Diamond Relat. Mater.* **126**, 109082 (2022)
[45] J Zhou, W Zhou, C Guan, J Shen, C Ouyang, M Lei and W Tang, *Sci. Chin. Phys. Mech. Astron.* **55**, 1376 (2012)
[46] F Wang, G Chen, W Li, Y Wang, C Wang, Y Zhang and Y Xia, *Adv. Mater. Interfaces* **3**, 1500496 (2016)
[47] R P Smith, T E Weller, C A Howard, M P Dean, K C Rahnejat, S S Saxena and M Ellerby, *Physica C: Supercond. Appl.* **514**, 50 (2015)
[48] J Wan, S D Lacey, J Dai, W Bao, M S Fuhrer and L Hu, *Chem. Soc. Rev.* **45**, 6742 (2016)
[49] J Han, D Kang and J Dai, *RSC Adv.* **8**, 19732 (2018)
[50] M-M Otrokov, I-I Klimovskikh, F Calleja, A-M Shikin, O Vilkov, A-G Rybkin and A Arnau, *2D Mater.* **5**, 035029 (2018)
[51] J-D Bernal, *Proc. R. Soc. Lond. A* **106**, 749 (1924)
[52] J-C Slater, *Phys. Rev.* **82**, 538 (1951)
[53] O-K Andersen, *Phys. Rev. B* **12**, 3060 (1975)
[54] P Blaha, K Schwarz, G K H Madsen, D Kuasnicke and J Luitz, *Vienna University of Technology, Vienna, Austria*, **60**(1) (2001)
[55] F Tran and P Blaha, *Phys. Rev. Lett.* **102**, 226401 (2009)
[56] J-P Perdew, K Burke and M Ernzerhof, *Phys. Rev. Lett.* **77**, 3865 (1996)
[57] S Hassine, O Farkad, F Elfatouaki, R Takassa, A El Mouncharih, O Choukri and D Abouelaoualim, *Mater. Sci. Semicond. Process.* **166**, 107725 (2023)
[58] A-S Olayinka, O-E Odeyemi and T-C Olayinka, *Jordan J. Phys.* **14**, 255 (2021)
[59] F Elfatouaki, R Takassa, O Farkad, S Hassine, O Choukri, A El Mouncharih and D Abouelaoualim, *Mater. Today Sustainability* **24**, 100572 (2023)
[60] F-D Murnaghan, *Proc. Natl. Acad. Sci.* **30**, 244 (1944)
[61] M Kumar, *Physica B* **212**, 391 (1995)
[62] L-M Malard, M-H Guimarães, D-L Mafra and A Jorio, *Phys. Rev. B* **79**, 125426 (2009)
[63] E Lee and K-A Persson, *Nano Lett.* **12**, 4624 (2012)
[64] S-Y Sheu and D-Y Yang, *Carbon* **71**, 76 (2014)
[65] C Tayran, S Aydin, M Cakmak and Ş Ellialtıoğlu, *Solid State Commun.* **231**, 57 (2016)
[66] M L Ould Ne, M Boujnah, A Benyoussef and A E Kenz, *J. Supercond. Novel Magn.* **30**, 1263 (2017)
[67] J Hargrove, H-M Shashikala, L Guerrido, N Ravi and X-Q Wang, *Nanoscale* **4**, 4443 (2012)
[68] W Yao, E Wang, C Bao, Y Zhang, K Zhang, K Bao and S Zhou, *Proc. Natl. Acad. Sci.* **115**, 6928 (2018)
[69] K-S Novoselov, D Jiang, F Schedin, T-J Booth, V-V Khotkevich, S-V Morozov and A-K Geim, *Proc. Natl. Acad. Sci.* **102**, 10451 (2005)
[70] T Ohta, A Bostwick, T Seyller, K Horn and E Rotenberg, *Science* **313**, 951 (2006)
[71] K Ji, J Han, A Hirata, T Fujita, Y Shen, S Ning and Y Oyama, *Nat. Commun.* **10**, 275 (2019)
[72] M-S Alam, J Lin and M Saito, *Jpn. J. Appl. Phys.* **50**, 080213 (2011)
[73] R Sharma, S Khan, V Goyal, V Sharma and K-S Sharma, *Flat. Chem.* **1**, 20 (2017)
[74] N-V Petrova and I-N Yakovkin, *Surf. Rev. Lett.* **24**, 1750020 (2017)
[75] M Pivetta, F Patthey, I Barke, H Hovel, B Delley and W-D Schneider, *Phys. Rev. B* **71**, 165430 (2005)
[76] M-D Williams, D-K Samarakoon, D-W Hess and X-Q Wang, *Nanoscale* **4**, 2962 (2012)
[77] M Gajdoš, K Hummer, G Kresse, J Furthmüller and F Bechstedt, *Phys. Rev. B* **73**, 045112 (2006)
[78] S-L Adler, *Phys. Rev.* **126**, 413 (1962)
[79] N Wiser, *Phys. Rev.* **129**1, 62 (1963)
[80] S Brodersen, D Lukas and W Schattke, *Phys. Rev. B* **66**, 085111 (2002)
[81] S Hassine, O Farkad, R Takassa, F Elfatouaki, O Choukri, Y Ijdiaou and D Abouelaoualim, *Rev. Mex. Fis.* **69**, 041002-1 (2023)
[82] P Nath, D Sanyal and D Jana, *Curr. Appl. Phys.* **15**, 691 (2015)
[83] A Laref, M Alsagri, S M Alay-e-Abbas, S Laref, H M Huang, Y C Xiong and X Wu, *Optik* **206**, 163755 (2020)
[84] T Gharbi, D Barchiesi, S Kessentini and R Maalej, *Opt. Mater. Express* **10**, 1129 (2020)
[85] S Nomura, Y Morimoto, H Tsujimoto, M Arake, M Harada, D Saitoh and H Ueno, *Sci. Rep.* **10**, 9765 (2020)